Int J Fract (2015) 194:45–50
DOI 10.1007/s10704-015-0028-z

BRIEF NOTE

Solution for a crack stiffened by an elliptic layer in antiplane elasticity

Y. Z. Chen

Received: 14 November 2014 / Accepted: 2 June 2015 / Published online: 18 June 2015

Abstract This paper provides a solution for a crack stiffened by elliptic layer in antiplane elasticity. The crack is embedded in an elliptic region and stiffened by a confocally elliptic layer. The whole medium is composed of three portions, the cracked elliptic plate, the confocally elliptic layer and the infinite matrix. The remote loading is applied. The cracked elliptic plate and the infinite matrix have the same shear modulus of elasticity. The stiffening elliptic layer has a higher shear modulus of elasticity. By using the complex variable and the continuity conditions along interfaces, the problem can be solved. One numerical example with different sizes and properties of materials is given to show the effect of the stiffening layer.

Keywords Stress intensity factors · Crack in inclusion · Stiffening problem for crack · Complex variable method · Antiplane elasticity

1 Introduction

Many stiffening problems for the cracked components were proposed (Isida 1973; Chen 1994; Umamaheswar and Singh 1999; Duong and Yu 1997; Antipov et al. 1997). The tension problem of a long cracked strip with stiffened edges was investigated (Isida 1973). The tension problem of a finite cracked plate with stiffened edges was studied (Chen 1994). Two contact problems referring to the partially stiffened elastic half-plane were studied (Antipov et al. 1997).

The problem of assessing the effectiveness of a bonded repair to a cracked plate can be reduced to a one-dimensional integral equation for the special case when both the plate and the reinforcement are isotropic and have the same Poisson's ratio (Wang and Rose 1998). Bonded composite repairs are efficient and cost effective means of repairing cracks and corrosion grind-out cavity in metallic structures (Duong and Wang 2007). Fundamental concept of crack patching was studied. The crack growth behavior of an aluminum plate cracked at the tip and repaired with a bonded boron/epoxy composite patch in the case of full-width disbond was investigated (Errouane et al. 2014). A numerical model for the optimization of composite patch repair of aluminum plate containing a central crack was developed (Errouane et al. 2014).

On the other hand, many researchers studied the antiplane problem for the elastic elliptic inclusion or layers (Gong 1995; Ru and Schiavone 1996; Chao and Young 1998; Shen et al. 2006; Chen and Wu 2007; Chen 2013). A generalized and unified treatment was presented for the antiplane problem of an elastic elliptic inclusion undergoing uniform eigenstrains and subjected to arbitrary loading in the surrounding matrix (Gong 1995). A novel efficient procedure to analyze the two-phase confocally elliptic inclusion embedded

Y. Z. Chen (✉)
Division of Engineering Mechanics, Jiangsu University, Zhenjiang 212013, Jiangsu, People's Republic of China
e-mail: chens@ujs.edu.cn

in an unbounded matrix under antiplane loadings was provided (Shen et al. 2006). Dual null-field integral equations was suggested for the multi-inclusion problem under antiplane shears (Chen and Wu 2007). A closed form solution for the Eshelby's elliptic inclusion in antiplane elasticity was provided (Chen 2013). The interaction problem between a circular inclusion and a symmetrically branched crack embedded in an infinite elastic medium was solved (Lam et al. 1998). A crack problem for an array of collinear microcracks in composite matrix was investigated (Profant and Kotoul 2005). It is found that most previously published papers in the solution for confocally elliptic layers were devoted to a perfect inclusion without crack.

This paper provides a solution for a crack stiffened by elliptic layer in antiplane elasticity. The crack is embedded in an elliptic region and stiffened by a confocally elliptic layer. The whole medium is composed of three portions, the cracked elliptic plate, the confocally elliptic layer and the infinite matrix. The remote loading is denoted by σ_{yz}^{∞}. The cracked elliptic plate and the infinite matrix have the same shear modulus of elasticity. The stiffening elliptic layer has a higher shear modulus of elasticity. By using the complex variable and the continuity conditions along interfaces, the problem can be solved. One numerical example with different sizes and properties of materials is given to show the effect of the stiffening layer.

2 Analysis

For convenience in derivation, we make a substitution $\phi(z) = -i\psi(z)$ in (Chen et al. 2003) and obtain the following complex potential for antiplane elasticity

$$\psi(z) = -f(x, y) + iGw(x, y) \tag{1}$$

where G is the shear modulus of elasticity, w(x, y) is the longitudinal displacement in antiplane elasticity. In addition, the result force function f(x, y) is defined by

$$f(x, y) = \int_{z_o}^{z} (\sigma_{xz}dy - \sigma_{yz}dx) \tag{2}$$

In Eq. (2), the integration is performed from a fixed point z_o to a moving point "z". In addition, σ_{xz} and σ_{yz} denote two stress components. Clearly, the displacement component w(x,y) and the resultant force function f(x,y) satisfy the following Laplace equation

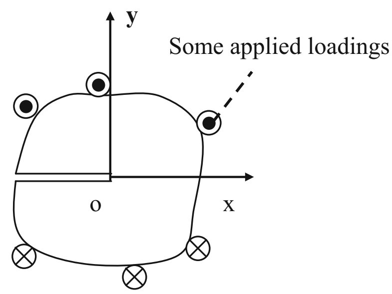

Fig. 1 An edge crack problem in antiplane elasticity

$$\nabla^2 w(x, y) = 0, \ \nabla^2 f(x, y) = 0 \text{ where}$$
$$\nabla^2 = \frac{\partial^2}{\partial x^2} + \frac{\partial^2}{\partial y^2} \tag{3}$$

From Eqs. (1) to (3), we can define the stress components by

$$\psi'(z) = \sigma_{yz} + i\sigma_{xz} = -\frac{\partial f}{\partial x} + iG\frac{\partial w}{\partial x} = G\left(\frac{\partial w}{\partial y} + i\frac{\partial w}{\partial x}\right) \tag{4}$$

In addition, from Eq. (1) we can get the following equations

$$2Gw(x, y) = -i(\psi(z) - \overline{\psi(z)}) \tag{5}$$

$$f(x, y) = -\frac{1}{2}(\psi(z) + \overline{\psi(z)}) \tag{6}$$

For an edge crack shown in Fig. 1, the stress intensity factor at the crack tip can be defined by (Chen et al. 2003)

$$K_3 = \lim_{z \to 0} \sqrt{2\pi z}\,\psi'(z) \tag{7}$$

It was proved that, the right hand term of Eq. (7) generally takes a real value in general (Chen et al. 2003).

If the stresses σ_{xz}^{∞} and σ_{yz}^{∞} are applied at infinity for an infinite medium, from Eq. (4) the relevant complex potential is as follows

$$\psi(z) = (\sigma_{yz}^{\infty} + i\sigma_{xz}^{\infty})z \tag{8}$$

For the crack embedded in an elliptic plate in antiplane elasticity, the following mapping function is used (Muskhelishvili 1953)

$$z = \omega(\varsigma) = \frac{a}{2}\left(\varsigma + \frac{1}{\varsigma}\right) \tag{9}$$

which maps the unit circle and its exterior region in the ς-plane into the crack configuration $(-a, a)$ and its exterior region in the z-plane. The cracked medium is

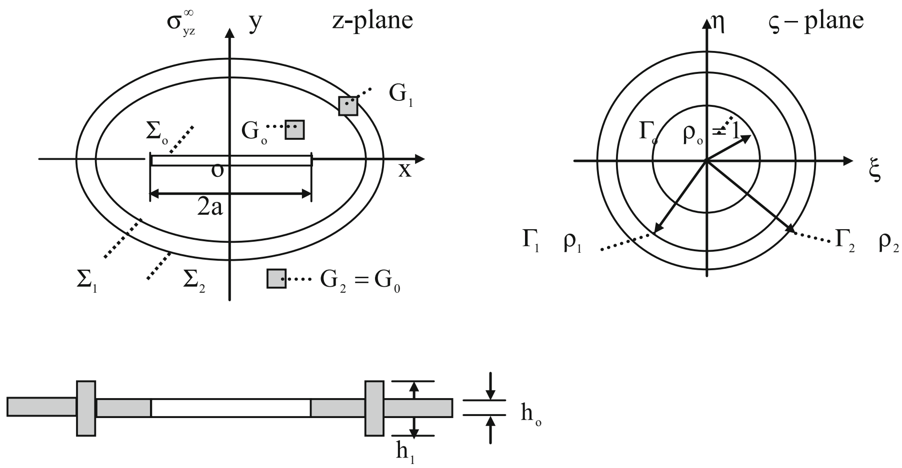

Fig. 2 Mapping relations for $z = \omega(\varsigma) = \frac{a}{2}(\varsigma + \frac{1}{\varsigma})$, (a) Ring region bounded by Γ_o (with $\rho_o = 1$) and Γ_1 in the ς-plane into the corresponding elliptic region bounded by Σ_o[crack along $(-a\ a)$] and Σ_1 in the z-plane, (b) Ring region bounded by Γ_1 with ρ_1 and Γ_2 with ρ_2 in the ς- plane into the corresponding elliptic layer bounded by Σ_1 and Σ_2 in the z-plane and (c) Infinite region exterior to Γ_2 with ρ_2 in the ς-plane into the corresponding infinite region exterior to Σ_2 in the z-plane

composed of (a) a cracked elliptic plate bounded by Σ_o [crack along $(-a\ a)$] and Σ_1, (b) an elliptic layer bounded by Σ_1 and Σ_2 and (c) an infinite region exterior to the contour Σ_2 (Fig. 2).

The mapping function also provides the following mappings: (a) it maps the circle Γ_o (with $\varsigma = \rho_o e^{i\theta}$ and $\rho_o = 1$) in the ς-plane into a crack configuration Σ_o [along the interval $(-a, a)$] in the z-plane, (b) it maps circles Γ_j (with $\varsigma = \rho_j e^{i\theta}$, $j=1, 2$) in the ς-plane into contours Σ_j $(j=1, 2)$ in the z-plane (Fig. 2).

In the formulation (Fig. 2), the layer bounded by Σ_1 and Σ_2 is thicker than other portions. In this case, we can assume the layer possesses a higher shear modulus of elasticity. However, if the layer bounded by Σ_1 and Σ_2 is a dissimilar material with a different modulus of elasticity, the derivation in this case is the same as in the studied case.

In addition, the shear modulus of elasticity for confocally elliptic layer bounded Σ_j and Σ_{j+1} is denoted by G_j $(j=0, 1)$. The shear modulus of elasticity for the medium exterior to Σ_2 is denoted by G_2 (Fig. 2). In this case, we have G_o, $G_1 = h_1 G_o/h_o$ and $G_2 = G_o$ for different portions, respectively (Fig. 2).

The inverse of the mapping function of $z = \omega(\varsigma)$ is denoted by

$$\varsigma = \Omega(z) = \frac{1}{a}(z + \sqrt{z^2 - a^2}) \tag{10}$$

Clearly, for $\varsigma \in \Gamma_{j+1}$, or $\varsigma = \rho_{j+1} e^{i\theta}$ $(j= -1, 0, 1)$, from Eq. (9) we have

$$\varsigma\bar{\varsigma} = \rho_{j+1}^2, \quad \left(\varsigma \in \Gamma_{j+1}, \ \text{or}\ \varsigma = \rho_{j+1} e^{i\theta}\right) \tag{11}$$

$$\overline{\omega(\varsigma)} = \frac{a}{2}\left(\frac{\varsigma}{\rho_{j+1}^2} + \frac{\rho_{j+1}^2}{\varsigma}\right), \quad \left(\varsigma \in \Gamma_{j+1}, \text{or}\ \varsigma = \rho_{j+1} e^{i\theta}\right) \tag{12}$$

Eq. (12) reveals that along the boundary $\varsigma \in \Gamma_{j+1}$, or $\varsigma = \rho_{j+1} e^{i\theta}$, the function $\overline{\omega(\varsigma)}$ can be converted into the form of an analytic function.

If the remote loading is σ_{xz}^{∞} only, the stress intensity factor K_3 always equal to zero. Therefore, we only study the case of the remote loading σ_{yz}^{∞}.

The complex potentials defined on many confocally elliptic layers bounded by $\Sigma_j$and Σ_{j+1} $(j = 0, 1)$ are denoted by $\psi_j^*(z)$ $(j = 0, 1)$. The complex potential defined exterior to the Σ_2 is denoted by $\psi_2^*(z)$ (Fig. 2).

Based on those complex potentials $\psi_j^*(z)$ $(j = 0, 1, 2)$, we can define the following complex potentials in the ς-plane as follows

$$\psi_j(\varsigma) = \psi_j^*(z)\,|_{z=\omega(\varsigma)}, \quad (j = 0, 1.2) \tag{13}$$

Clearly, the displacement and traction and along the interface $\varsigma \in \Gamma_{j+1}$ $(j = 0, 1)$ should be continuous. Therefore, from Eqs. (1), (5) and (6) we can propose the continuity conditions along the interfaces $\varsigma \in \Gamma_{j+1}$ $(j = 0, 1)$ as follows

$$\frac{1}{G_{j+1}}(\psi_{j+1}(\varsigma) - \overline{\psi_{j+1}(\varsigma)}) = \frac{1}{G_j}(\psi_j(\varsigma) - \overline{\psi_j(\varsigma)}), \ (\varsigma \in \Gamma_{j+1}, \ j = 0, \ 1) \quad (14)$$

$$\psi_{j+1}(\varsigma) + \overline{\psi_{j+1}(\varsigma)} = \psi_j(\varsigma) + \overline{\psi_j(\varsigma)}, \ (\varsigma \in \Gamma_{j+1}, \ j = 0, 1) \quad (15)$$

Eq. (14) is derived Eq. (5), which represents the displacement continuity condition along interfaces. In addition, Eq. (15) is derived Eq. (6), which represents the traction continuity condition along interfaces. It is easy to verify that the traction continuity condition along interfaces is equivalent to the same condition for resultant force "f" shown in Eq. (1). Thus, the equality shown by Eq. (15) is obtained.

The complex potentials for the cracked elliptic plate, confocal layer and infinite matrix are expressed in the form

$$\psi_j(\varsigma) = c_j\varsigma + d_j\frac{1}{\varsigma}, \ (j = 0, 1, 2 \text{ with } c_j, \ d_j \text{ real value}) \quad (16)$$

From Eqs. (14) to (16), we can link the two sets of two undetermined coefficients in the adjacent layers as follows

$$c_{j+1} = \alpha_j c_j - \frac{\beta_j}{\rho_{j+1}^2} d_j,$$
$$d_{j+1} = -\rho_{j+1}^2 \beta_j c_j + \alpha_j d_j, \ (j = 0, \ 1) \quad (17)$$

where

$$\alpha_j = \frac{G_{j+1} + G_j}{2G_j}, \quad \beta_j = \frac{G_{j+1} - G_j}{2G_j}, \ (j = 0, 1) \quad (18)$$

We prefer to write Eq. (17) in an explicit form

$$c_1 = \alpha_0 c_0 - \frac{\beta_0}{\rho_1^2} d_0, \quad d_1 = -\rho_1^2 \beta_0 c_0 + \alpha_0 d_0 \quad (19)$$

$$c_2 = \alpha_1 c_1 - \frac{\beta_1}{\rho_2^2} d_1, \quad d_2 = -\rho_2^2 \beta_1 c_1 + \alpha_1 d_1 \quad (20)$$

On the other hand, from Eqs. (1), (6) and (16), we can propose the traction free condition along the crack face

$$\psi_o(\varsigma) + \overline{\psi_o(\varsigma)} = 0, \ (\text{for } \varsigma \in \Gamma_o, \text{ or } \varsigma = e^{i\vartheta}) \quad (21)$$

From Eq. (16) we can express the complex potential $\psi_o(\varsigma)$ as follows

$$\psi_o(\varsigma) = c_o\,\varsigma + \frac{d_o}{\varsigma} \quad (22)$$

Substituting Eq. (22) into (21) yields

$$d_o = -c_o, \text{ or } \psi_o(\varsigma) = c_o\varsigma - \frac{c_o}{\varsigma} \quad (23)$$

Since $\psi_2^*(z) = \sigma_{yz}^\infty z + O(1/z)$ and $z \approx a\varsigma/2$ at the remote place, from Eqs. (9) and (16) we will find

$$c_2 = \frac{a}{2}\sigma_{yz}^\infty \quad (24)$$

and

$$\psi_2(\varsigma) = c_2\varsigma + d_2\frac{1}{\varsigma} = \frac{a}{2}\sigma_{yz}^\infty\varsigma + d_2\frac{1}{\varsigma}, \quad (25)$$

In the formulation, there are six unknowns, or c_o, d_o, c_1, d_1, c_2, d_2. In the meantime, we also have six equations for six unknowns: (1) four equations from Eqs. (19) and (20), representing the continuity conditions along two interfaces Σ_1 and Σ_2, (2) $d_o = -c_o$ from Eq. (23), representing the traction free condition along the crack face and (3) $c_2 = \frac{a}{2}\sigma_{yz}^\infty$ from Eq. (24), representing the remote loading condition. Finally, we can obtain six undetermined coefficients.

In addition, from Eq. (7) the stress intensity factor at the crack tip can be defined by

$$K_3 = \lim_{\varsigma \to 1} \sqrt{2\pi(\omega(\varsigma) - a)}\frac{\psi_0'(\varsigma)}{\omega'(\varsigma)}, \ (\text{with } a = \omega(1)) \quad (26)$$

Subsisting Eq. (23) into (26) yields

$$K_3 = \frac{2c_o}{a}\sqrt{\pi\, a} \quad (27)$$

3 Numerical example

In the case of the remote loading σ_{yz}^∞, one numerical example is provided to show the influence to stress intensity factor K_3 from (a) the area of the thicker portion and (b) the assumed ratio for the shear modulus G_1/G_o under the condition $G_2 = G_o$.

In the example, the mapping function $z = \omega(\varsigma) = \frac{a}{2}(\varsigma + \frac{1}{\varsigma})$ shown by Eq. (9) is used (Fig.2). In addition, we define the following three parameters. The first parameter δ is defined by

$$\delta = \frac{\rho_1}{\rho_o}, \ (\text{with } \rho_o = 1, \text{ or } \delta = \rho_1) \quad (28)$$

The second parameter is used for defining the relation of ρ_2 to $\delta = \rho_1$. The semi-axes corresponding to $\rho_j (j = 1, 2)$ are denoted by a_j and $b_j (j = 1, 2)$. It is assumed that the area bounded by Σ_1 and Σ_2 (Fig. 2) keeps a definite value. In this case we can define second parameter α by

$$\alpha = \frac{\pi(a_2b_2 - a_1b_1)}{\pi a^2} = \frac{a_2b_2 - a_1b_1}{a^2} \tag{29}$$

Clearly, from the mapping function shown by Eq. (9), we have

$$\begin{matrix} a_1 \\ b_1 \end{matrix} = \frac{a}{2}\left(\rho_1 \pm \rho_1^{-1}\right), \quad \begin{matrix} a_2 \\ b_2 \end{matrix} = \frac{a}{2}\left(\rho_2 \pm \rho_2^{-1}\right) \tag{30}$$

Substituting (30) into (29) yields

$$\alpha = \frac{1}{4}\left((\rho_2^2 - \rho_2^{-2}) - (\rho_1^2 - \rho_1^{-2})\right), \text{ or } (\rho_2^2 - \rho_2^{-2}) = 4\alpha + (\rho_1^2 - \rho_1^{-2}) \tag{31}$$

Eq. (31) reveals that if α and ρ_1 are given beforehand, we can get ρ_2 from Eq. (31) accordingly. In the example, we choose $\alpha = 0.25$ or 0.5.

Finally, the third parameter γ is defined by

$$\gamma = \frac{G_1}{G_o} \tag{32}$$

In the example, we choose $G_2 = G_o$.

In the example, we assume (1) $\delta = \rho_1/\rho_o$= 1.01, 1.02, 1.05, 1.1. 1.2, 1.5, 2, 5 (with $\rho_o = 1$), (2) $\gamma = G_1/G_o$ =1, 2, 3, 4, 5, 8, 10 and (3) $\alpha = 0.25, 0.5$. After using Eq. (27), the computed results for K_3 at the crack tip can be expressed as

$$K_3 = h(\delta, \gamma, \alpha)\sigma_{yz}^{\infty}\sqrt{\pi a} \tag{33}$$

The computed non-dimensional stress intensity factors $h(\delta, \gamma, \alpha)$ are listed in Table 1.

From Table 1 we see that, the γ value ($\gamma = G_1/G_o$) has a significant influence to the non-dimensional stress intensity factors (SIFs) $h(\delta, \gamma, \alpha)(= K_3/(\sigma_{yz}^{\infty}\sqrt{\pi a}))$. For example, in the case of $\alpha = 0.25$, we have $h(\delta, \gamma, \alpha)\,|_{\delta=1.01\,\gamma=1} = 1.000$ and $h(\delta, \gamma, \alpha)\,|_{\delta=1.01\,\gamma=5} = 0.571$. That is to say, if the thickness of elliptic layer is magnified by five time, the non-dimensional SIF is reduced from 1 to 0.571. Similarly, the δvalue ($\delta = \rho_1/\rho_o$) also has a significant influence to the non-dimensional stress intensity factors (SIFs) $h(\delta, \gamma, \alpha)(= K_3/(\sigma_{yz}^{\infty}\sqrt{\pi a}))$. For example, in the case of $\alpha = 0.25$, we have $h(\delta, \gamma, \alpha)\,|_{\delta=2\gamma=1} = 1.000$, $h(\delta, \gamma, \alpha)\,|_{\delta=2\,\gamma=2} = 0.960$ and $h(\delta, \gamma, \alpha)\,|_{\delta=2\,\gamma=5} = 0.825$. That is to say, if the stiffening layer is far away ($\delta = 2$ case) from the crack tip, the reduction of the non-dimensional SIF is not significant.

Table 1 The non-dimensional stress intensity factors $h(\delta, \gamma, \alpha)$ $(= K_3/(\sigma_{yz}^{\infty}\sqrt{\pi a}))$ at the crack tip with $\delta = \rho_1/\rho_o (\rho_o = 1)$, $\gamma = G_1/G_o$, $G_2 = G_o$ [see Eq. (33) and Fig. 2]

γ / δ	1	2	3	4	5	8	10
$h(\delta, \gamma, \alpha)$ values in the case of $\alpha = 0.25$							
1.01	1.000	0.842	0.727	0.639	0.571	0.432	0.371
1.02	1.000	0.845	0.730	0.643	0.574	0.435	0.375
1.05	1.000	0.852	0.740	0.654	0.586	0.446	0.385
1.1	1.000	0.863	0.756	0.672	0.604	0.464	0.402
1.2	1.000	0.882	0.784	0.705	0.639	0.500	0.436
1.5	1.000	0.924	0.850	0.785	0.728	0.597	0.533
2	1.000	0.960	0.912	0.867	0.825	0.720	0.663
5	1.000	0.995	0.986	0.977	0.968	0.942	0.925
$h(\delta, \gamma, \alpha)$ values in the case of $\alpha = 0.5$							
1.01	1.000	0.777	0.635	0.536	0.464	0.331	0.278
1.02	1.000	0.780	0.639	0.541	0.468	0.335	0.281
1.05	1.000	0.790	0.650	0.553	0.480	0.345	0.290
1.1	1.000	0.804	0.669	0.572	0.499	0.361	0.305
1.2	1.000	0.830	0.703	0.608	0.535	0.394	0.335
1.5	1.000	0.885	0.781	0.697	0.628	0.483	0.418
2	1.000	0.934	0.861	0.795	0.737	0.604	0.538
5	1.000	0.990	0.974	0.958	0.941	0.894	0.864

In addition, in the case of $\alpha = 0.5$, we have $h(\delta, \gamma, \alpha)\,|_{\delta=1.01\,\gamma=1} = 1.000$ and $h(\delta, \gamma, \alpha)\,|_{\delta=1.01\,\gamma=5} = 0.464$. That is to say, the thickness of elliptic layer is magnified by five time, the non-dimensional SIF is reduced from 1 to 0.464. Similarly, in the case of $\alpha = 0.5$, we have $h(\delta, \gamma, \alpha)\,|_{\delta=2\,\gamma=1} = 1.000$, $h(\delta, \gamma, \alpha)\,|_{\delta=2\,\gamma=2} = 0.934$ and $h(\delta, \gamma, \alpha)\,|_{\delta=2\,\gamma=5} = 0.737$. That is to say, if the stiffening layer is far away ($\delta = 2$ case) from the crack tip, the reduction of the non-dimensional SIF is minor.

Except for the $\gamma = G_1/G_o = 1$ case, the non-dimensional SIFs in the case of $\alpha = 0.5$ are generally lower than those for the case of $\alpha = 0.2$.

4 Conclusions

Generally, the continuity conditions along interfaces in the problem is rather complicated. We found that we only need to express the complex potentials in the form of Eq. (16). Therefore, the two sets of two undetermined coefficients in the adjacent layers can be linked by Eq. (17).

This paper provides an effective solution for a crack stiffened by elliptic layer in antiplane elasticity. A lot of numerical results are provided in this paper. It is found that if the stiffening layer is placed near the crack tip, for example, $\rho_1 = 1.01$, the stiffening effect is significant. However, if the stiffening layer is placed far away from the crack tip, for example $\rho_1 = 5$, the stiffening effect is weaker.

This paper provides a closed form solution for the mentioned crack problem. In fact, after substituting the relations $d_o = -c_o$ and $c_2 = \frac{a}{2}\sigma_{yz}^{\infty}$ shown by Eqs. (23) and (24) into Eqs. (19) and (20), we will obtain an algebraic equation for four unknowns c_o, c_1, d_1 and d_2. This algebraic equation is indeed a very simple one, and no error is actually involved in computation. Thus, the computed results achieved must be very high.

References

Antipov YA, Bardzokas D, Exadaktylos GE (1997) Partially stiffened elastic half-plane with an edge crack. Int J Fract 85:241–263

Chao CK, Young CW (1998) On the general treatment of multiple inclusions in antiplane elastostatics. Int J Solids Struct 35:3573–3593

Chen JT, Wu AC (2007) Null-field approach for the multi-inclusion problem under antiplane shears. J Appl Mech 74:469–487

Chen YZ (1994) Tension of a finite cracked plate with stiffened edges. Eng Fract Mech 49:667–670

Chen YZ (2013) Closed form solution for Eshelby's elliptical inclusion in antiplane elasticity using complex variable. Z Angew Math Phys 69:1797–1805

Chen YZ, Hasebe N, Lee KY (2003) Multiple crack problems in elasticity. WIT Press, Southampton

Duong CN, Yu J (1997) The stress intensity factor for a cracked stiffened sheet repaired with an adhesively bonded composite patch. Int J Fract 84:37–60

Duong CN, Wang CH (2007) Composite repair theory and design. Elsevier Science, Amsterdam

Errouane H, Sereir Z, Chateauneuf A (2014) Numerical model for optimal design of composite patch repair of cracked aluminum plates under tension. Inter J Adhes Adhes 49:64–72

Gong SX (1995) A unified treatment of the elastic elliptical inclusion under antiplane shear. Arch Appl Mech 65:55–64

Isida M (1973) Method of Laurent series expansion for internal crack problems. In: Sih GC (ed) Mechanics of Fracture, vol 1. Springer, Netherlands, pp 56–130

Lam KY, Ong PP, Wude N (1998) Interaction between a circular inclusion and a symmetrically branched crack. Theo Appl Fract Mech 28:197–211

Muskhelishvili NI (1953) Some basic problems of mathematical theory of elasticity. Noordhoff, Groningen

Profant T, Kotoul M (2005) On collinear microcrack-inclusions arrays interaction and related problems. Theo Appl Fract Mech 44:297–328

Ru CQ, Schiavone P (1996) On the elliptic inclusion in anti-plane shear. Math Mech Solids 1:327–333

Shen MH, Chen SN, Chen FM (2006) Antiplane study on confocally elliptical inhomogeneity problem using an alternating technique. Arch Appl Mech 75:302–314

Umamaheswar TVRS, Singh R (1999) Modelling of a patch repair to a thin cracked sheet. Eng Fract Mech 62:267–289

Wang CH, Rose LRF (1998) Bonded repair of cracks under mixed mode loading. Inter J Solids Struct 35:2749–2773